W. J. Jasinski
Graduate Research Assistant.

S. C. Noe[1]
Graduate Research Assistant.

M. S. Selig
Assistant Professor.

M. B. Bragg
Professor.

Department of Aeronautical and Astronautical Engineering,
University of Illinois at Urbana-Champaign,
306 Talbot Laboratory,
104 S. Wright Street
Urbana, IL 61801-2935

Wind Turbine Performance Under Icing Conditions

The effects of rime ice on horizontal axis wind turbine performance were estimated. For typical supercooled fog conditions found in cold northern regions, four rime ice accretions on the S809 wind turbine airfoil were predicted using the NASA LEWICE code. The resulting airfoil/ice profile combinations were wind tunnel tested to obtain the lift, drag, and pitching moment characteristics over the Reynolds number range $1-2 \times 10^6$. These data were used in the PROPID wind turbine performance prediction code to predict the effects of rime ice on a 450-kW rated-power, 28.7-m diameter turbine operated under both stall-regulated and variable-speed/variable-pitch modes. Performance losses on the order of 20 percent were observed for the variable-speed/variable-pitch rotor. For the stall-regulated rotor, however, a relatively small rime ice profile yielded significantly larger performance losses. For a larger 0.08c-long rime ice protrusion, however, the rated peak power was exceeded by 16 percent because at high angles the rime ice shape acted like a leading edge flap, thereby increasing the airfoil $C_{l,max}$ and delaying stall.

Introduction

For many northern regions of the world, the best locations for the placement of wind energy stations are along coastal areas or on the tops of hills and mountains. These locations, however, are inherently susceptible to atmospheric icing events during the winter months. Performance degradation of horizontal axis wind turbines (HAWTs) due to ice accretion has been investigated on a number of machines at different locations (Rong and Bose, 1990; Seifert and Schloz, 1990; Chappell and Templin, 1985; Bose, 1992b; Rong, et al., 1991; Seifert, 1992). Power output can be negligible for a wind turbine operating under extreme icing conditions. In fact, using noniced control tables the wind turbine will most likely not even start. Furthermore, random shedding of ice from the rotating turbine blades can cause severe out-of-balance loads on the wind turbine. These added loads increase material fatigue, reducing the operational life of the turbine and causing nonproductive downtimes for repair.

Icing concerns regarding wind turbine operation are not limited to extreme icing conditions but start at the first sign of surface roughness on the blades. It has been shown that even the slightest amount of surface roughness has the potential to reduce energy output from a wind turbine by 20 percent (Rong and Bose, 1990). As the icing process continues, aerodynamic performance degradation is similar to that experienced by aircraft wings (Chappell and Templin, 1985) and helicopter rotors (Bose, 1992b).

Methods of ice prevention, similar to those applied to aircraft, have been investigated for wind turbine use (Chappell and Templin, 1985; Bose, 1992b). As Makkonen and Autti (1991) conclude for a 100-kW turbine, however, "anti-icing by heating requires at least 25 percent of the maximum power production capacity of the turbine, and the energy required for efficient deicing by sudden heating far exceeds this capacity." For smaller wind turbines, the problem of ice prevention is even more severe because of (1) the lower potential power output as compared with a larger turbine and (2) the higher ice-collection efficiency or "impingement efficiency," which represents the dimensionless mass flux of impinging droplets at a point on the airfoil surface. Regarding the latter, for fixed-size droplets approaching an airfoil with a short chord on a small wind turbine, the amount of droplet impingement is increased because the droplets experience the streamline curvature only once quite close to the airfoil. The streamline curvature is therefore greater than for a larger chord airfoil. Consequently, as the airfoil chord becomes shorter, the droplets approaching the airfoil leading edge deviate more from the local streamlines and result in a greater amount of direct impingement as compared with a longer chord airfoil.

For more severe icing events, stopping the turbine may be the most logical solution owing to the energy required for ice prevention and wear on the machine. Stopping a wind turbine during the presence of every icing condition, however, would be nonproductive. For slight to moderate icing events, where the turbine continues to operate but at reduced levels of efficiency, it may be beneficial to continue operation with or, perhaps, without anti-icing devices in place. The determination of the best option to maximize energy output from the turbine operating in an icing environment requires a knowledge of the performance loss that can be expected during the icing event.

To predict the degradation in wind turbine performance due to icing, wind tunnel tests were conducted under clean and various icing conditions. The S809 wind turbine airfoil (Tangler and Somers, 1995) (see Fig. 1) was chosen for this study. Lift, drag, and pitching moment data were taken over the Reynolds number range of $1-2 \times 10^6$. The icing conditions studied included initial ice accretions and four rime ice accretions that were determined using the NASA LEWICE code (Ruff, 1990). The airfoil wind tunnel test data were then used in the strip-theory code PROPID (Selig and Tangler, 1995) to predict the effects of ice accretions on wind turbine performance.

Experimental Methods

The experiments were performed at the University of Illinois at Urbana-Champaign (UIUC) Low-Turbulence Subsonic Wind Tunnel. The tunnel is a conventional open-return type with a contraction ratio of 7.5:1. Test section dimensions are approximately 0.853 × 1.219 m, widening approximately 1.27 cm over the 2.43-m length of the test section to allow for boundary layer growth. The tunnel inlet settling chamber contains 10.16-cm thick honeycomb followed by four antiturbulence screens. Test section flow velocity can be varied up to 71.52

[1] Currently Engineer, Hughes Missile Systems Co., Tucson, AZ 85734.

Contributed by the Solar Energy Division of THE AMERICAN SOCIETY OF MECHANICAL ENGINEERS for publication in the ASME JOURNAL OF SOLAR ENERGY ENGINEERING. Manuscript received by the ASME Solar Energy Division, Jan. 1997; final revision, Mar. 1997. Associate Technical Editor: P. S. Veers.

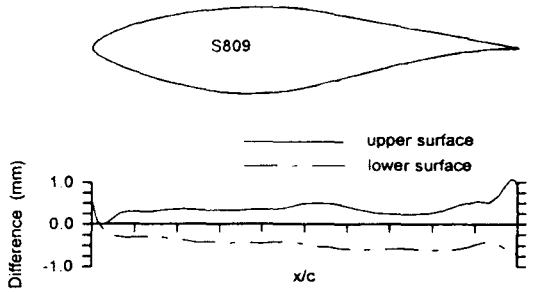

Fig. 1 Comparison between the NREL S809 model coordinates and true coordinates

m/s (160 mph), which corresponds to a Reynolds number of approximately 4.9×10^6/m.

The two-dimensional S809 airfoil model was cantilevered vertically in the tunnel and spanned the test section height. The 0.457-m chord model was constructed of a carbon-fiber skin surrounding a foam core. Steel pipe spars were used at the 20 percent and 60 percent chord stations and attached to the balance force plate through a flange. To ensure that the model did not touch the tunnel walls, the model was fixtured to allow for a gap of approximately 0.5 mm at the balance (floor) and 0.9 mm at the free end (ceiling).

To determine the profile accuracy of the model, the contour was digitized with a Brown & Sharpe coordinate measuring machine. The measured coordinates at the model centerline were compared with the true coordinates using a two-dimensional least squares approach (rotation and vertical translation). Figure 1 shows the comparison of the S809 measured model coordinates (dot-dash line) and true coordinates (solid line). The figure depicts the differences between the model airfoil and the true airfoil upper surface (solid line) and lower surface (dot-dash line). A displacement above or below the axis means that the model surface lies above or below the true, respectively. Thus, the S809 was thicker than the true airfoil by approximately 0.39 mm over most of the upper and lower surface airfoil chord.

Airfoil lift and moment data were taken with a three-component external floor-mounted balance manufactured by Aerotech ATE Limited of Heathfield, UK. The normal and axial forces measured by the balance were used to determine the lift force. The pitching moment was also measured by the balance. Drag data over the low drag range (typically -7 to 8 deg) was determined by the standard wake momentum deficit method reported by Jones (1936) and described in Schlichting (1979). Three total-head pressure probes spaced 7.62 cm apart were traversed horizontally through the wake (perpendicular to the model span) at 3.8-mm intervals. The center probe approximately corresponded to the center of the model. Pressures were acquired using a Pressure Systems, Inc. 8400 electronically scanned pressure system with ± 6.9 kPa (± 1 psid) and ± 34.5 kPa (± 5 psid) pressure scanners. For angles of attack higher than approximately 8 deg, drag data used later in the wind turbine performance prediction section were taken from balance measurements.

Lift, drag, and moment data taken on the S809 model for Re $= 1.5 \times 10^6$ are shown in Fig. 2 and compared with data taken at Delft (Somers, 1989) and The Ohio State University (OSU) (Ramsay et al., 1994). Although there are some differences, particularly at the corners of the polar, the agreement shown is good, and this serves to validate the current approach (Noe, 1996).

Icing Conditions and Simulation

The model was tested with simulated initial and rime ice accretions based on predictions that were determined using the NASA-Lewis LEWICE code (Version 1.6) (Ruff, 1990). In the model, any unfrozen water runs back on top of the frozen water layer in a uniform wet film. This runback provides the mechanism for glaze ice formation in the code, but it is at odds with recent experimental studies of glaze ice accretion physics (Hansman, 1993; Olsen and Walker, 1986). However, for rime ice for which the temperatures are so low that the freezing occurs quickly with little runback, LEWICE predicts ice accretion accurately (Bragg et al., 1996).

The particular icing conditions considered are listed in Table 1. In the table, LWC refers to the liquid water content. These ground icing conditions are representative of those experienced by the primary airfoil (75 percent blade-radius station) of a typical 450-kW wind turbine in operation during supercooled fog/cloud conditions (hereafter simply referred to as supercooled fog). Supercooled fog conditions, which give rise to rime ice accretions, mainly occur along coastal regions and/or mountain peaks in the northwestern U.S., Alaska, Greenland, and valleys in western Europe. Rime ice accretions on wind turbines are particularly problematic in some regions of Finland where conditions for rime ice can last 20–25 consecutive days (Tammelin and Säntti, 1992). (Such long icing conditions cannot be modeled using LEWICE.) In the current study, the principal parameters varied included the accretion time and droplet size. The resulting ice profiles shown in Fig. 3 are typical of rime ice profiles seen on wind turbines under such conditions.

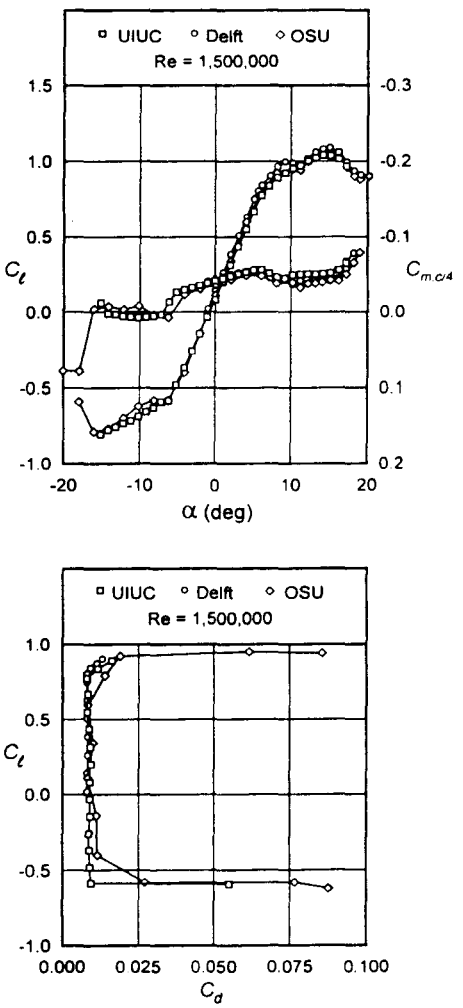

Fig. 2 Comparison of the NREL S809 measured drag polars from the UIUC, Delft (Somers, 1989) and Ohio State (Ramsey et al., 1994) wind tunnel facilities

Table 1: Icing conditions corresponding to the four rime ice profiles (R1, R2, R3, and R4).

Droplet Dia. (μm)	Icing event duration (hr) 3	7
15	R1	R2
35	R3	R4
Conditions for supercooled fog		
$\alpha = 5$ deg $c = 0.75$ m $V = 65.2$ m/s		
$T = -10$ deg C LWC= 0.1 g/m^3		

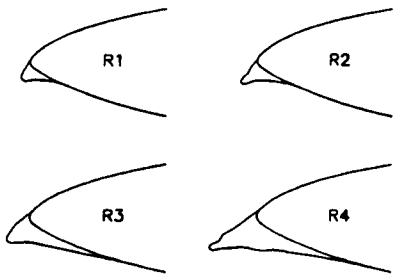

Fig. 3 Illustration of the four leading-edge rime ice profiles tested (only 20 percent of chord shown)

The onset of ice accretion (light rime ice) was simulated by applying aluminum oxide grit over the model leading edge, referred to as leading-edge grit roughness (LEGR). The limits of simulated accretion were $x/c = 0.005$ on the upper surface and $x/c = 0.05$ on the lower. Two different degrees of roughness were simulated by using 46 and 16-grit aluminum oxide, which corresponded to k/c values of 0.0009 and 0.0019, respectively, where k is the nominal grit diameter. The approximate grit densities for the initial ice accretions were 62/cm^2 for $k/c = 0.0009$ and 2.3/cm^2 for $k/c = 0.0019$. These grit densities and sizes were selected on the basis that they approximately simulated the trends observed for initial ice accretion, in particular, the trend that as accretion times increase the roughness size is increased while the density is decreased.

Simulated rime ice accretions for the profiles shown in Fig. 3 were manufactured from foam-cores covered with carbon-fiber skins. These ice profiles were secured to the model leading edge with tape along the span and screws at the end cap ribs. Again, 46 and 16-grit aluminum oxide was used to simulate the rime ice roughness; however, due to the more lengthy ice accretion times, the grit densities were increased to approximately 155/cm^2 for $k/c = 0.0009$ and 13/cm^2 for $k/c = 0.0019$. The grit in this case was only applied to the rime ice profile.

Test Results

In this section, highlights of the airfoil performance data are presented and discussed. Figure 4 shows the $C_l - \alpha$, $C_l - C_{m,c/4} - \alpha$ and $C_l - C_d$ curves for Re = 1×10^6 and 2×10^6. Data are shown for the airfoil under clean conditions, with leading-edge grit roughness (LEGR) and with ice profiles R2 and R4 for $k/c = 0.0019$. It should be noted that the coefficients

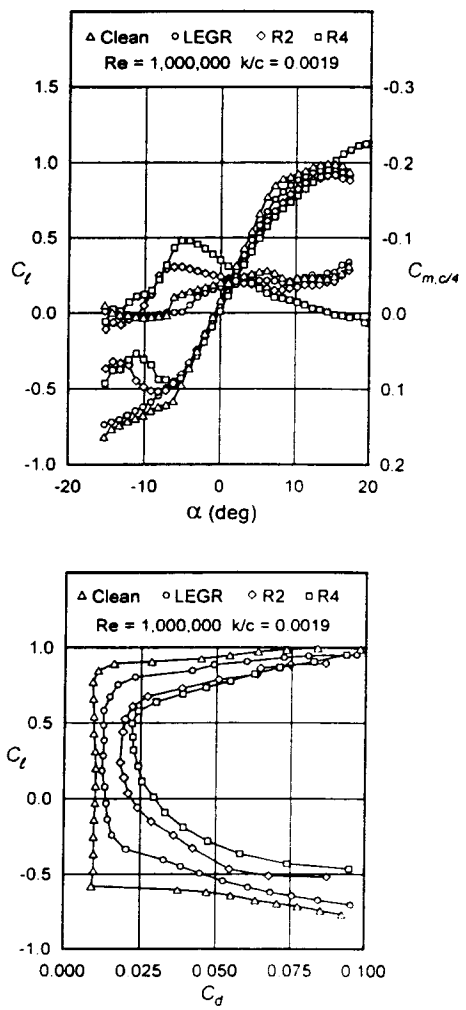

Fig. 4 S809 performance for Re = 1×10^6 and 2×10^6 under clean and icing conditions for $k/c = 0.0019$

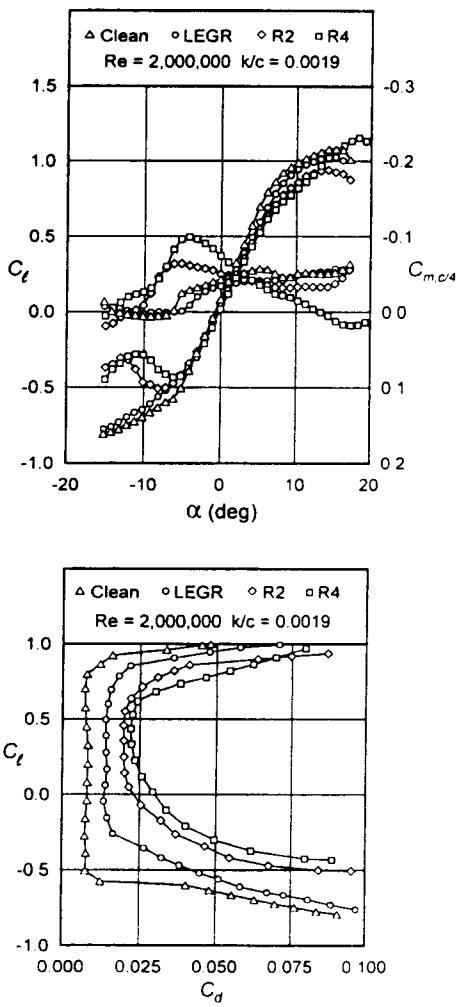

Fig. 4 (cont'd)

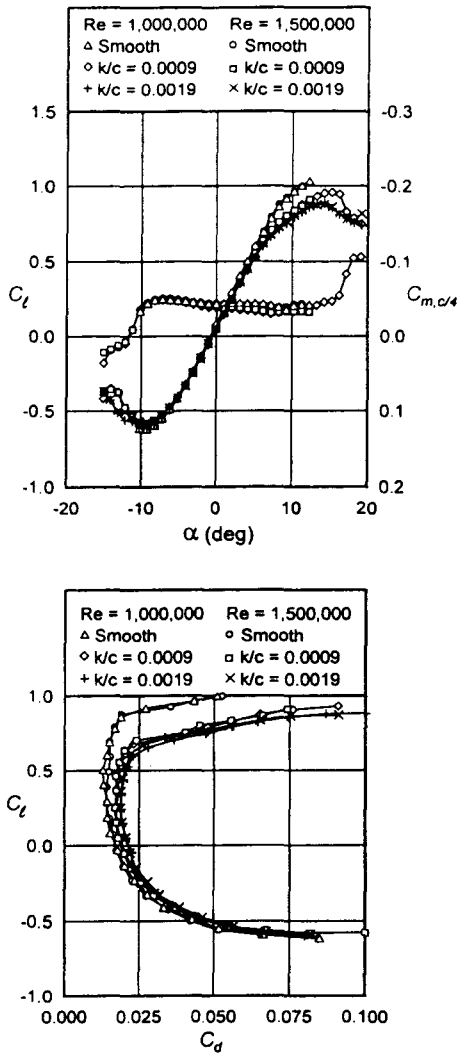

Fig. 5 The effects of roughness on the S809 for Re = 1 × 10^6 and 1.5 × 10^6 ice profile R1

are normalized by the nominal airfoil chord, that is, the chord length of the original clean section. If the data for the ice profiles were normalized by the airfoil chord including the rime ice horn, the corresponding coefficients would be reduced by 2.5 percent and 7.2 percent for cases R2 and R4, respectively.

The two most obvious features of the polars are the large loss in lift and the increase in drag as the degree of icing increases. It is particularly noticeable that the lowest drag for the icing cases corresponds to the angle of attack used to generate the ice profiles, that is, $\alpha = 5$ deg ($C_l \approx 0.5$ for case R4 at Re = 1 × 10^6)—a result that is typical of other tests on iced airfoils. Above and below this angle of attack, significant flow separation occurs on the upper and lower surfaces, respectively. The result is an increase in drag above and below the 5 deg angle of attack. The sharp rise in drag above 5 deg is caused by the rapid growth of upper surface separation, which is also reflected in the change in the lift curve slope.

Several other interesting features can be identified. First, Fig. 4 illustrates important Reynolds number effects. As expected, the drag was reduced with increasing Reynolds number for the clean case. For the icing cases, however, the Reynolds number effects were minimal because transition to turbulent flow was promoted artificially by the grit roughness—a process that is known to be rather insensitive to Reynolds number for large roughness. Second, the rather dramatic increase in $C_{l,max}$ and stall delay for ice profile R4 as compared with the clean case and the other icing cases is surprising. It is, however, similar to the effects produced by leading-edge flaps (McCormick, 1995) and by ice shapes that mimic the effect (Bragg et al., 1982). Third, as the icing becomes more extreme, the separation pocket on the lower surface at zero lift grows, thereby producing a slight increase in the zero-lift angle of attack. Finally, the pitching moment curves change rather dramatically as compared with the clean case. This trend is most easily explained by considering the R4 case. As the angle of attack is increased, the pitching moment becomes more positive, which is indicative of a center of pressure that moves forward. This movement is attributable to the large upper-surface leading-edge suction peak, which becomes more extreme with increasing angle of attack.

Additional tests were performed to determine the effect of roughness on the ice shapes. The results shown in Fig. 5 for case R1 at Re = 1 × 10^6 and 1.5 × 10^6 are quite typical of the other cases. When the roughness is reduced from k/c = 0.0019 to 0.0009, there is a small drag reduction. When no roughness is used, however, drag is substantially reduced, and the low drag range is extended to higher lift coefficients. These changes result from less separated flow as can be deduced from the increase in lift over the entire positive lift range. Clearly, these results underscore the importance of simulating the roughness of the rime ice.

Effects of Rime Ice on HAWT Performance

The experimental data were used in the strip-theory code, PROPID (Selig and Tangler, 1995), to estimate the effects of the rime ice on the power production of a 28.7-m diameter three-blade rotor operated in both stall-regulated and variable-speed/variable-pitch modes. For both cases, the rotor blade depicted in Fig. 6 was designed for a rated power of 450 kW under clean conditions. For the stall-regulated case, a rotor speed of 48 rpm was used with a blade pitch of 1.36 deg toward feather. A tip-speed ratio of 7 was used for the variable-speed/variable-pitch case, and the pitch was again 1.36 deg.

Figure 7(a) shows the predicted performance for the stall-regulated rotor for the clean case and for rime ice cases R2 and R4 with k/c = 0.0019. Corresponding data are shown in Fig. 7(b) for the variable-speed/variable-pitch rotor. It is known that for the variable-speed/variable-pitch rotors in operation at constant tip-speed ratio, the C_l-distribution along the blade span remains the same for wind speeds below that for rated power. Thus, the percentage loss in performance due to icing is nearly constant at all wind speeds—14.5 percent for rime ice profile R2 and 20 percent for R4. It is worth noting that above the rated wind speed, the power output is unaffected. Thus, for a site with average wind speeds near the rated wind speed, the energy loss from icing becomes less important.

For the stall-regulated rotor, the lift coefficient along the blade span changes with wind speed, and this leads to substantially different effects as compared with the variable-speed/

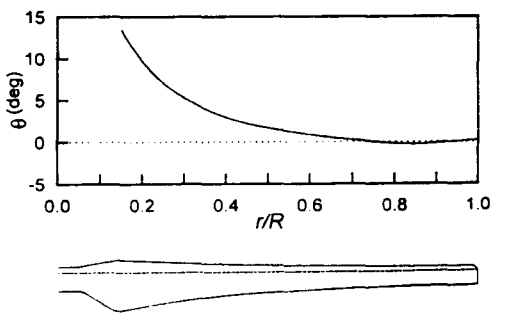

Fig. 6 Rotor geometry used to study the effects of rime ice accretion on wind turbine performance

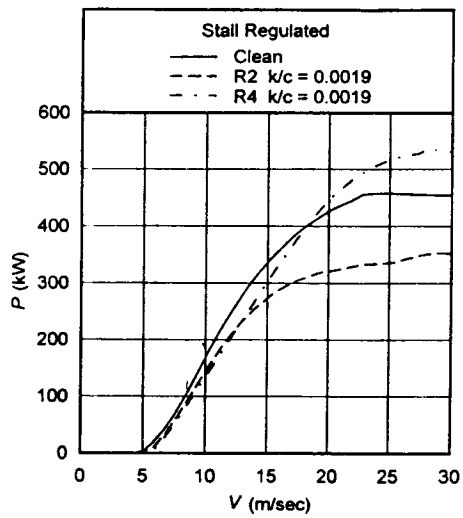

Fig. 7(a)

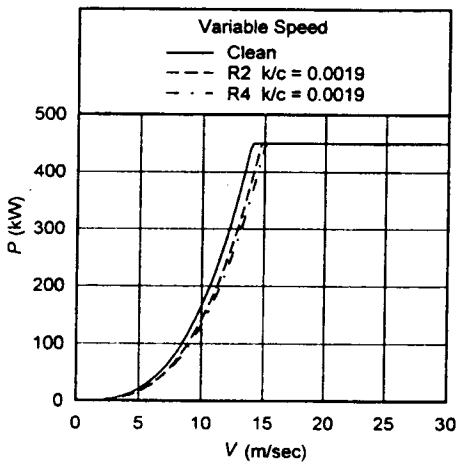

Fig. 7(b)

Fig. 7 Rotor performance under clean and icing conditions for operation in the (a) stall-regulated and (b) variable-speed/variable-pitch modes

variable-pitch case. For wind speeds above approximately 13 m/s, the power curves are dictated largely by the airfoil characteristics in the vicinity of stall. In particular, a higher $C_{l,\max}$ produces a higher peak rotor power. For rime ice profile R2, the $C_{l,\max}$ is below that for the clean airfoil (see Fig. 4). Consequently, the power curve falls below that for the clean case. Both the loss in lift and increase in drag lead to the substantial loss in peak rotor power. For rime ice profile R4, however, the airfoil $C_{l,\max}$ is increased over the clean case and the stall is delayed to a higher angle of attack—effects that are produced by the streamlined rime ice profile that acts similar to a leading-edge flap. Thus, for rime ice profile R4, there is a rather large increase in peak power, which unfortunately leads to greater generator and blade loads. This result provides supporting evidence to speculation that ice buildup has been responsible for stall delay and associated peak power excursions on wind turbines in icing environments (Ronsten, 1993). It should be added, however, that such events are rare, and they may be caused not by increased lift but rather increased air density at the low temperatures. Below 13 m/s where the blade is largely unstalled, the performance degradation is similar to that for the variable-speed/variable-pitch rotor. An interesting difference, however, is the undesirable increased cut-in speed, which is caused by the stall-regulated blade suffering a greater loss in the blade L/D distribution at startup as compared with the variable-speed/variable-pitch case that operates at a higher lift coefficient distribution at startup.

It should be noted that the estimated performance under icing conditions is based on using the measured iced airfoil performance data along the entire span. The icing condition corresponds approximately to that experienced by the blade at the 75 percent station. Toward the blade tip, the ice accretion would be higher than that tested and likewise lower than tested toward the root, as has been observed (Bose, 1992a). Thus, these two competing effects will tend to offset each other, making the use of a single data set representative of the conditions at the 75 percent station appropriate.

Conclusions

Horizontal axis wind turbines located in northern regions along coastlines and atop high mountains where winds are generally favorable for wind energy production are susceptible to rime ice accretion under supercooled fog and cloud conditions. The resulting adverse effects on wind turbine performance were estimated by using experimental data acquired on the S809 wind turbine airfoil under typical rime icing conditions. Based on the results for variable-speed/variable-pitch rotors, the performance degraded uniformly by as much as 20 percent at wind speeds below rated power, while above the rated wind speed no loss occurred. For the stall-regulated rotors that rely on airfoil stall to regulate power, the effects of rime ice can be more pronounced and unexpected. As shown, a small rime horn that protruded $0.025c$ ahead of the clean airfoil leading edge led to a loss in performance over the entire operating range, especially at wind speeds near peak power. In contrast, a larger $0.08c$-long rime ice horn behaved like a leading-edge flap and produced an increase in $C_{l,\max}$ and a delay in stall to a higher angle of attack. These changes in the airfoil performance led to a 16 percent increase in the peak rotor power—an undesirable result that can lead to generator burnout and high blade loads. Finally, these estimates are conservative since the ice accretion studied here did not attempt to model the extreme icing events sometimes observed on real rotors under more prolonged rime ice conditions.

Acknowledgments

The support of the National Renewable Energy Laboratory under Subcontract XAF-4-14076-03 is gratefully acknowledged. Also, the several discussions with James L. Tangler of NREL proved to be quite helpful during the course of this work. Assistance from R. Chrenko of Kenetech Windpower and R. K. Jeck of the FAA Technical Center in identifying the conditions under which icing took place on wind turbines is gratefully acknowledged.

References

Bragg, M. B., Gregorek, G. M., and Shaw, R. J., 1982, "Wind Tunnel Investigation of Airfoil Performance Degradation Due to Icing," AIAA Paper 82-0582, Mar.

Bragg, M. B., Cummings, M. J., Lee, S., and Henze, C. M., 1996, "Boundary-Layer and Heat-Transfer Measurements on a Airfoil with Simulated Ice Roughness," AIAA Paper 96-0866, Jan.

Bose, N., 1992a, "Icing on a Small Horizontal Axis Wind Turbine—Part 1: Glaze Ice Profiles," *J. of Wind Engineering and Industrial Aerodynamics*, Vol. 45, pp. 75–85.

Bose, N., 1992b, "Icing on a Small Horizontal Axis Wind Turbine—Part 2: Three Dimensional Ice and Wet Snow Formations," *J. of Wind Engineering and Industrial Aerodynamics*, Vol. 45, pp. 87–96.

Chappell, M. S., and Templin, R. J., 1985, "And the Cold Winds Shall Blow . . . Wind Energy Research and Development in Canada—Spring 1985," *Proceedings of the 7th British Wind Energy Association Conference*, Oxford, UK.

Hansman, R. J., 1993, "Microphysical Factors which Influence Ice Accretion," *Proceedings of the First Bombardier International Workshop on Aircraft Icing/Boundary-Layer Stability and Transition*, L. Paraschivoiu, ed., Ecole Polytechnique, Montreal, Quebec, Canada, Sept. 20–21, pp. 86–103.

Jones, B. M., 1936, "The Measurement of Profile Drag by the Pitot Traverse Method," Aeronautical Research Council, R&M 1688.

Makkonen, L., and Autti, M., 1991, "The Effects of Icing on Wind Turbines," *Proceedings of the European Community Wind Energy Conference*, Amsterdam, Netherlands.

McCormick, B. W., 1995, *Aerodynamics, Aeronautics, and Flight Mechanics*, 2nd Ed., John Wiley and Sons, Inc., New York.

Noe, S. C., 1996, "Force Balance Measurements of Wind-Turbine Airfoil Performance with Simulated Leading-Edge Ice Accretions," Master's thesis, University of Illinois at Urbana-Champaign, Urbana, IL, Aug.

Olsen, W., and Walker, E., 1986, "Experimental Evidence for Modifying the Current Physical Model for Ice Accretion on Aircraft Surfaces," NASA TM-87184, Lewis Research Center, Cleveland, OH.

Rong, J. Q., and Bose, N., 1990, "Power Reduction from Ice Accretion on a Horizontal Axis Wind Turbine," *Proceedings of the 12th British Wind Energy Association Conference*, Norwich, UK, Mar. 27–30.

Rong, J. Q., Bose, N., Brothers, C., and Lodge, M., 1991, "Icing Test on a Horizontal Axis Wind Turbine," *Wind Engineering*, Vol. 15, No. 2, pp. 109–113.

Ronsten, G., 1993, "Can Delayed Stall Be Caused by Ice Accretion on the Leading Edge of an Airfoil?," FFA Institute of Sweden, FFAP-A-981, Stockholm, Sweden, May.

Ruff, G., 1990, "Users Manual for the NASA Lewis Ice Accretion Prediction Code (LEWICE)," NASA CR-185129, May.

Schlichting, H., 1979, *Boundary-Layer Theory*, 7th Ed; McGraw-Hill, New York.

Seifert, H., and Schloz, C., 1990, "Additional Loads Caused by Ice on Rotor Blades During Operation," *Proceedings of the European Community Wind Energy Conference*, Madrid, Spain, Sept. 10–14.

Seifert, H., 1992, "Icing of Wind Turbine Rotor Blades During Operation," presented at BOREAS, An International Expert's Meeting on Wind Power in Icing Conditions, Enontekiö, Finland.

Selig, M. S., and Tangler, J. L., 1995, "Development and Application of a Multipoint Inverse Design Method for Horizontal Axis Wind Turbines," *Wind Engineering*, Vol. 19, No. 2, pp. 91–105.

Somers, D. M., 1989, "Design and Experimental Results for the S809 Airfoil," Airfoils, Inc., Hampton, VA, Mar.

Tammelin, B., and Säntti, K., 1992, "Rime Accretions on the Fells," presented at BOREAS, An International Expert's Meeting on Wind Power in Icing Conditions, Enontekiö, Finland.

Tangler, J. L., and Somers, D. M., 1995, "NREL Airfoil Families for HAWTs," *Proceedings of the American Wind Energy Association WINDPOWER Conference*, Washington, D.C., Mar.

Ramsay, R. R., Hoffmann, M. J., and Gregorek, G. M., 1994, "Effects of Grit Roughness and Pitch Oscillation on the S809 Airfoil," Draft Report of The Ohio State University, Aeronautical and Astronautical Research Laboratory, Columbus, OH, National Renewable Energy Laboratory Contract No. XF-1-11009-3, June.

Wright, W. B., and Potapczuk, M. G., 1996, "Computational Simulation fo Large Droplet Icing," Proceedings of the FAA Interational Conference on Aircraft Inflight Icing, Vol. II, Report No. DOT/FAA/AR-96/81, II, Aug., pp. 545–555.